Optical pumping of Rb in the presence of high-pressure ^{3}He buffer gas

B. Larson
Simon Fraser University, Burnaby, British Columbia, Canada V5A 1S6

O. Häusser
Simon Fraser University, Burnaby, British Columbia, Canada V5A 1S6
and TRIUMF, 4004 Wesbrook Mall, Vancouver, British Columbia, Canada V6T 2A3

P. P. J. Delheij, D. M. Whittal, and D. Thiessen
TRIUMF, 4004 Wesbrook Mall, Vancouver, British Columbia, Canada V6T 2A3
(Received 12 April 1991)

A cryogenic technique has been used to produce polarized ^{3}He targets of up to relative density $p=12$ atm ($\approx 3\times10^{20}$ ^{3}He atoms/cm^3; $p=1$ atm corresponds to 760 Torr or 101.3 kPa pressure at 273 K). In these targets ^{3}He nuclei are polarized by spin-exchange collisions with optically pumped rubidium atoms. From transmission measurements at wavelengths of 790–800 nm, we have determined pressure shifts, linewidths, and line-shape asymmetries for the Rb $5S_{1/2}\rightarrow 5P_{1/2}$ $D1$ transition. The Rb spin-destruction rate was found to exhibit a quadratic increase versus ^{3}He pressure, which indicates the importance of Rb-^{3}He-^{3}He collision processes. The transmission results for circularly polarized light are well described by a model that predicts the dependence of the average Rb polarization on Rb density, ^{3}He pressure, light intensity, and cell geometry. The Rb-^{3}He spin-exchange cross section, $\langle\sigma_{SE}v\rangle=6.1\times10^{-20}$ cm^{3}s^{-1}, was found to be independent of ^{3}He pressure up to $p=12.1$ atm. Maximum ^{3}He polarizations of 72–79 % were observed with cells of 17 cm^3 volume that contained ^{3}He at $p=6$–9 atm.

I. INTRODUCTION

The polarization of the nuclear spin of ^{3}He is of interest from several perspectives. Applications of polarized ^{3}He in atomic physics, surface physics, and quantum statistics have been discussed in a recent review by Leduc [1]. The motivation for the present work was the production of polarized ^{3}He targets for applications in nuclear and particle physics. To a good approximation polarized ^{3}He can be viewed as a polarized neutron. The two protons are predominant in a spatially symmetric S state, with the unpaired neutron carrying about 90% of the nuclear spin [2]. Quasielastic and deep inelastic scattering of longitudinally polarized electrons from polarized ^{3}He can provide information on the electric and magnetic form factors of the ^{3}He nucleus [3] and on the internal spin structure of the neutron. The strong interaction of slow neutrons with polarized ^{3}He has been used as a spin filter for neutron beams [4]. Experiments in which intermediate-energy protons and pions are scattered from polarized ^{3}He determine largely unexplored spin-dependent scattering amplitudes and probe details of the three-body nucleonic wave function of ^{3}He. Such experiments are presently being pursued at TRIUMF.

Forcible nuclear orientation methods using low temperatures ($\simeq 5$ mK) and large magnetic fields ($\simeq 5$ T) have achieved sizable polarizations in solid ^{3}He [5]. The large magnetic fields and low heat capacity of the solid make these targets of limited use for applications in nuclear and particle physics. The only practical methods employed at present are optical pumping, i.e., the absorption of polarized light by the atom, and transfer of the atomic polarization to the nucleus by the hyperfine interaction. In the optical pumping of metastable ^{3}He the $2\,^3S_1-2\,^3P$ transition of helium is pumped by $\lambda=1.08$-μm light and the polarization is transferred from the metastable to the ground state by metastablity exchange collisions [6]. The low ^{3}He density associated with producing metastables in a weak discharge can be overcome using cryogenic storage cells [7]. At present such targets satisfy the luminosity demands of experiments in nuclear and particle physics if large currents ($\gg 1$ μA) of primary internal or external beams are available.

Experiments with weak primary, or with even weaker secondary, beams require $>10^{21}$ polarized ^{3}He target nuclei, 1–2 orders of magnitude more than has been achieved so far with metastable optical pumping. Targets of the necessary figure of merit (which can be defined as the product of areal density times polarization squared) can be produced using optical pumping of alkali metals and polarization transfer from the alkali metal to ^{3}He via spin-exchange collisions. This method, which was discovered by Bouchiat, Carver, and Varnum [8] and studied further by Gamblin and Carver [9], is made possible by extremely long nuclear relaxation times T_1 of ^{3}He nuclei achievable in suitable containment cells. Calculations by Herman [10] confirmed that the spin-exchange cross sections are surprisingly large for ^{3}He and ^{21}Ne. Polarization of noble-gas nuclei by spin exchange has since been actively studied both experimentally and theoretically [11–16]. Using solid-state diode lasers or dye lasers capable of producing ~ 1 W of light output,

Chupp and collaborators [17,18] have achieved significant ^{3}He polarizations at high density ($p \approx 3$ atm) although the volumes of these targets were limited to only a few cm^3. With the advent of tuneable Ti:sapphire (Ti^{3+}:Al_2O_3) lasers 3–6 W of infrared light per laser system are now available for optical pumping of Rb or K vapor. Since the volume of Rb vapor which can be pumped to $\approx 100\%$ polarization increases linearly with the available laser power [17,18] much larger polarized target volumes can now be realized. For the present work a cryogenic technique has been developed at TRIUMP to increase the target density from $p = 3$ to 12 atm and the target volume to 35 cm^3. This development over the past two years has increased the figure of merit of the targets by more than an order of magnitude, which has made it possible to perform hadronic scattering experiments with external proton and pion beams at TRIUMF. A preliminary account of proton-scattering results obtained with these polarized targets can be found elsewhere [19].

The tunability and narrow linewidth (~ 18 GHz) of Ti:sapphire lasers makes them suitable for studying the pressure broadened line shape of the Rb $D1$ line. We present here measurements of the $D1$ line-shape parameters and of the Rb spin-destruction rates at various Rb densities and ^{3}He pressures between $p = 3$–12 atm. These properties must be known to predict the average Rb polarization and hence the maximum possible ^{3}He polarization. We have found a strong increase of the Rb spin-destruction rate Γ_{SD} with ^{3}He pressure which was unexpected and has a dramatic effect on the laser power per unit volume required to produce $\sim 100\%$ polarized Rb vapor at large ^{3}He pressures. We have also measured the pressure dependence of the cross section for Rb-^{3}He spin-exchange collisions and the rates for depolarization processes in the cell volume. These results and their discussion are presented in Sec. IV. They are preceded by a brief review of the theory of optical pumping and of spin exchange (see Sec. II). A description of the apparatus and experimental technique is given in Sec. III.

II. THEORY OF OPTICALLY PUMPED POLARIZED ^{3}He TARGETS

The polarization of ^{3}He nuclei involves the contact hyperfine interaction between the nuclear spin of ^{3}He and the atomic spin of the alkali metal (Rb) which is polarized by the optical pumping process. This interaction is effective during the brief time of Rb-^{3}He collisions. Since the time scales for polarization transfer (≈ 10 h) and for optical pumping of the alkali metal (≈ 1 ms) differ by seven orders of magnitude the steady-state ^{3}He polarization is directly proportional to P_{Rb}, the average alkali-metal polarization in the target volume, independent of the relative concentrations of alkali metal and ^{3}He. We shall show that transmission data for the alkali-metal $D1$ line for both linearly and circularly polarized light contain the information necessary to predict P_{Rb} reliably. In addition to its dependence on P_{Rb}, the ^{3}He polarization also depends on the ratio of rates for spin exchange and for depolarization processes in the volume. In our discussion we follow closely the notation of earlier work (see, e.g., Ref. [18]). The effect of the ^{85,87}Rb nuclear spins is neglected since the laser linewidth (≈ 18 GHz) far exceeds the Rb hyperfine splittings (3.04 and 6.87 GHz, respectively).

A. Absorption of linearly polarized light by Rb vapor

Linearly polarized (σ_0) laser light is absorbed by both $m_s = \pm\frac{1}{2}$ substates of the Rb $5s\ ^2S_{1/2}$ ground state. The absorption line-shape parameters can then be determined independent of the incident light intensity since the Rb vapor is always unpolarized. These parameters are then used to interpret the light transmission data obtained with circularly polarized light. The Rb volume is illuminated by a uniform, parallel beam of infrared photons of frequency ν. The intensity of the laser light after traversing a sample of thickness x is given by

$$\ln[I(0)/I(x)] = \sigma_\nu[\mathrm{Rb}]x = \kappa_\nu x \ , \tag{1}$$

where [Rb] is the rubidium number density, κ_ν is the inverse absorption length, and the cross section for absorption of a photon of wavelength λ_0 is

$$\sigma(\delta\nu) = \frac{\lambda_0^2}{8\pi}\Gamma_{\mathrm{nat}}\left[\frac{\Gamma}{(\delta\nu)^2+(\Gamma/2)^2} + \frac{b\,\delta\nu}{\Gamma}e^{-|\delta\nu|/\Gamma_a}\right] . \tag{2}$$

The first term in Eq. (2) describes a Lorentzian line shape which is symmetric with respect to the detuning parameter $\delta\nu = \nu - \nu_0(p)$. The total pressure broadened width Γ is much larger than the natural linewidth Γ_{nat} (5.66 MHz), the Doppler-broadened width (0.6 GHz), or the laser linewidth (18 GHz). In addition to pressure broadening, one observes a pressure shift of the resonance frequency, $\nu_0(p) - \nu_0(0)$, and an asymmetry in the line shape. The cause of these effects can be viewed [20,21] as a distortion of the Rb $5s\ ^2S_{1/2}$ and $5p\ ^2P_{1/2}$ atomic levels by the Rb-^{3}He interatomic potential. The second term in Eq. (2) is a convenient parameterization of the observed line-shape asymmetry, characterized by two new parameters b and Γ_a. It should be noted that this term does not contribute to the frequency integral of the cross section which is related to the $D1$ oscillator strength (f) via

$$\int_{-\infty}^{+\infty}\sigma d(\delta\nu) = \frac{\lambda_0^2}{4}\Gamma_{\mathrm{nat}} = \pi r_e c f \ , \tag{3}$$

independently of pressure broadening. For the allowed, strong electric dipole $D1$ transition it is safe to assume that the free values $\Gamma_{\mathrm{nat}} = (2\pi\tau)^{-1} = 5.66$ MHz and $f = 0.337$ are unchanged by the presence of the ^{3}He buffer gas. Since the asymmetric part of the absorption cross section is identically zero at the resonance frequency ($\delta\nu = 0$) the absorption maximum is unaffected by it. For more thorough discussions of the physics of pressure broadened line shapes we refer the reader to Refs. [20,21].

B. Polarization of Rb by absorption of circularly polarized light

Unlike linearly polarized $D1$ light which is absorbed by both magnetic substates of $5s\ ^2S_{1/2}$ Rb ground state, cir-

cularly polarized $\sigma_{\pm}$ light can be absorbed by the $m_s = \mp\frac{1}{2}$ substate only. The propagation of the σ_+ light intensity in the medium is described by the equation

$$\frac{dI_\nu^+(x)}{dx} = -2I_\nu^+ \sigma_\nu[\mathrm{Rb}]\rho_- \ , \tag{4}$$

where σ_ν is the cross section for scattering of linearly polarized light in unpolarized Rb vapor [Eq. (2)], and I_ν^+ is the intensity of circularly polarized σ_+ light incident on the sample. The m dependence of the transition probability accounts for the factor of 2. For ease of notation we define rates for circularly and linearly polarized photons, $\gamma_\nu^+ = I_\nu^+ \sigma_\nu$ and $\gamma_\nu^0 = I_\nu^0 \sigma_\nu$, respectively. Making use of the identity $\rho_+ = 1 - \rho_-$, we obtain the occupation probabilities ($\rho_\pm$) of the $m_s = \pm\frac{1}{2}$ substates from the time-dependent solution of the optical pumping rate equation:

$$\frac{d\rho_+(x)}{dt} = \left[\gamma_\nu^+(x) + \gamma_\nu^0(x) + \Gamma_{\mathrm{SD}} - D\frac{d^2}{dx^2}\right]\rho_-(x) - \left[\frac{\Gamma_{\mathrm{SD}}}{2} + \frac{\gamma_\nu^0(x)}{2}\right] = 0 \ . \tag{5}$$

The spin-destruction rate $\Gamma_{\mathrm{SD}} \approx \langle \sigma_{\mathrm{SD}} v \rangle [\mathrm{Rb}]$ has previously been assumed (see, e.g., Ref. [17]) to represent Rb depolarization in Rb-Rb ($\uparrow\uparrow \rightarrow \uparrow\downarrow$) collisions where σ_{SD} is the velocity averaged spin-destruction cross section. It will be shown that additional spin destruction arises from the presence of ^{3}He buffer gas. D, an effective diffusion constant for Rb atoms in ^{3}He gas, is introduced to account for differences in the Rb polarization near the cell boundary and in the uniform medium. A further assumption used in deriving the above rate equation is that collisional mixing in the excited ($5p\ ^2P_{1/2}$) state due to the presence of a small amount of N_2 quench gas results in 50% probabilities of deexcitation to the $m_s = -\frac{1}{2}$ and $m_s = +\frac{1}{2}$ substates of the ground state. We have calculated [22] the quenching factor for the Rb $D1$ line at a N_2 pressure of 120 Torr to be approximately equal to 50 using experimental quenching cross sections [23]. Numerical integration of Eq. (5) shows that the equilibrium polarizations $P(x) = \rho_+(x) - \rho_-(x)$ are attained about 1 ms after the laser light is switched on. The possibility that the light is elliptically polarized rather than circularly polarized is included in the γ^0 terms. We have found that the ellipticity of the laser light used for optical pumping can be made to be negligibly small (see Sec. III) and therefore disregard these terms in the following discussion.

The traditional method of determining the spin-destruction rate Γ_{SD} (see, e.g., Ref. [10]) consists of starting from unpolarized alkali-metal vapor, then illuminating the sample with light of a fixed frequency such that the light transmission grows exponentially from a finite small value to the equilibrium value. We have used here instead the steady-state solution of Eq. (5) and extracted Γ_{SD} from the detailed frequency dependence. The steady-state method is sensitive not only to Γ_{SD}, but also to depolarization effects at the cell walls which can easily be missed by the single-frequency time-dependent method.

In the steady state the propagation of the laser light can be followed through the sample numerically by solving the time-independent equations (4) and (5) at each value of x starting with the boundary condition $P_{\mathrm{Rb}} = 0$ at the cell wall, $x = 0$. The ansatz

$$P_{\mathrm{Rb}} = \beta(1 - e^{-\alpha x}) \tag{6}$$

is used to model the rapid buildup of the Rb polarization as a function of distance from the cell wall. The quantities $\rho_-(x) = \frac{1}{2}(1 - P_{\mathrm{Rb}})$ and $d^2\rho_-/dx^2$ can be written in terms of α and β,

$$\rho_-(x) = \tfrac{1}{2}(1 - \beta + \beta e^{-\alpha x}) \tag{7}$$

and

$$\frac{d^2\rho_-(x)}{dx^2} = \frac{\beta\alpha^2}{2} e^{-\alpha x} \ . \tag{8}$$

Substitution of these two quantities into the optical pumping rate equation (5) yields the required expressions for α and β,

$$\beta = \frac{\gamma_\nu^+}{\gamma_\nu^+ + \Gamma_{\mathrm{SD}}} \quad (x \rightarrow \infty) \tag{9}$$

$$\alpha = \left[\frac{\gamma_\nu^+ + \Gamma_{\mathrm{SD}}}{D}\right]^{1/2} \quad (x = 0) \ , \tag{10}$$

where $\beta \approx 1$ for all x if the incident light intensity is sufficiently high and α^{-1} gives the effective thickness of an unpolarized Rb layer that exists at the cell wall. One can then calculate $\alpha(x)$ and $\beta(x)$ at each x given the value of $\gamma_\nu^+(x)$ and subsequently determine $P_{\mathrm{Rb}}(x)$ where

$$P_{\mathrm{Rb}}(x) = \rho_+(x) - \rho_-(x) = \frac{\gamma_\nu^+(x)}{\gamma_\nu^+(x) + \Gamma_{\mathrm{SD}}} \times \left[1 - \exp - \left[\frac{\gamma_\nu^+(x) + \Gamma_{\mathrm{SD}}}{D}\right]^{1/2} x\right] . \tag{11}$$

Fitting the data obtained at a range of frequencies centered on the resonance frequency provides values for Γ_{SD}, the average Rb polarization, and the effective diffusion constant D. From Eq. (11) it is apparent that high Rb polarization requires the ratio of photon absorption rate γ_ν^+ to spin-destruction rate Γ_{SD} to be large.

C. Polarization transfer by spin-exchange collisions

The ^{3}He polarization ($\tilde{P}$) is given by $\tilde{\rho}_+ - \tilde{\rho}_-$ where $\tilde{\rho}_\pm$ is the probability of finding the ^{3}He nucleus with magnetic quantum number $m = \pm\frac{1}{2}$. The ^{3}He polarization is strongly dependent on three parameters: (i) the Rb polarization P_{Rb}, (ii) the velocity averaged spin-exchange cross section $\langle \sigma_{\mathrm{SE}} v \rangle$, and (iii) the wall relaxation rate of the cell Γ_w. The time evolution of the ^{3}He polarization is inferred from the rate equation

$$\frac{d\tilde{\rho}_+}{dt}=\left[\frac{\Gamma_w}{2}+\gamma_{SE}\rho_+\right]\tilde{\rho}_- - \left[\frac{\Gamma_w}{2}+\gamma_{SE}\rho_-\right]\tilde{\rho}_+ , \quad (12)$$

where $\gamma_{SE}=\langle\sigma_{SE}v\rangle[\mathrm{Rb}]$. With the substitution $\tilde{\rho}_-=1-\tilde{\rho}_+$, one obtains the solution

$$\tilde{P}(t)=P_{\mathrm{Rb}}\frac{\gamma_{SE}}{\gamma_{SE}+\Gamma_w}(1-e^{-(\gamma_{SE}+\Gamma_w)t}) \quad (13)$$

if the laser light is switched on at $t=0$, and

$$\tilde{P}(t)=\tilde{P}(0)e^{-(\gamma_{SE}+\Gamma_w)t} \quad (14)$$

if the laser is switched off at $t=0$. Equation (13) describes the optical pumping situation. High polarization is obtained when $P_{\mathrm{Rb}}\approx 1$ and $\gamma_{SE}\gg\Gamma_w$. Equation (14) describes the evolution of the ^{3}He polarization in the presence of unpolarized Rb vapor (laser off). As P_{Rb} does not appear in this equation, polarization decay at high temperature provides the most accurate means of determining $\gamma_{SE}+\Gamma_w$. Γ_w can be measured separately at low temperature where γ_{SE} is negligibly small.

III. EXPERIMENTAL TECHNIQUE

Polarized ^{3}He target cells produced at TRIUMF have been designed to meet the requirements of proton- and pion-scattering experiments. For proton beam experiments where the beam diameter is approximately 2 mm, target cells of 17-mm outer diameter and 8-cm length (volume ≈ 17 cm^3) are adequate. For experiments with secondary pion beams the beam diameter is much larger (2.5 cm full width at $\frac{1}{10}$ maximum) and larger diameter target cells are needed. Cells for pion applications have typically 26–29-mm outer diameter and a length of 8 cm (volume ≈ 35 cm^3).

Cells made of alumino-silicate glass (Corning 1720) are more resistant against reactions with alkali metal and exhibit longer wall relaxation times, Γ_w, than other types of glass. A schematic drawing of the setup used in making high density polarized ^{3}He target cells is displayed in Fig. 1. The target cell is connected by a thin capillary to a glass manifold also made of Corning 1720 glass. The manifold is pumped down to a pressure of $<5\times10^{-8}$ Torr and baked out at $T\approx 250$ °C for several days. A sealed glass ampule which contains the Rb metal is broken by the impact of a glass-coated steel ball and the Rb is subsequently chased by flame into the cell portion of the manifold. The system is then filled with ultrahigh purity ^{3}He gas which has passed through a tube immersed in liquid ^{4}He. The liquid helium acts as a cold trap for further purification of the ^{3}He gas. From the opposite side a few Torr of ultrahigh purity N_2 quench gas is added to the manifold contents. The N_2 gas passes through a trap cooled to 77 K by liquid N_2 for additional purification.

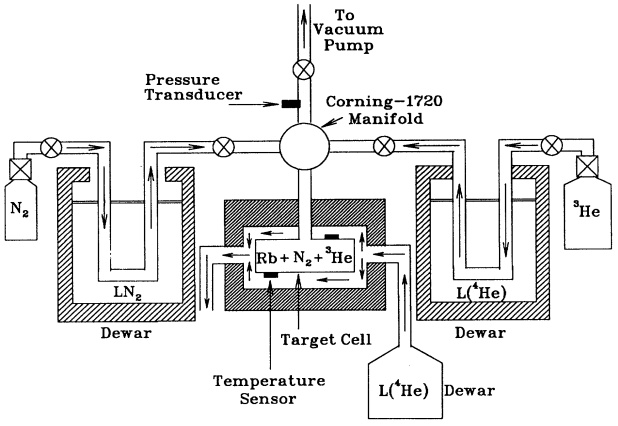

FIG. 1. Apparatus used to make target cells containing several standard atmospheres of ^{3}He gas, about 120 Torr of N_2 quench gas and Rb metal.

The manifold pressure is measured by a Baratron pressure transducer to an accuracy <1 Torr. The fraction f of the total volume that the cell occupies is determined by submerging the cell in liquid $N_2(T=77\ \mathrm{K})$ after the ^{3}He gas has been added, i.e.,

$$f=\left[\frac{p_R}{p_{77}}-1\right]\Big/\left[\frac{T_R}{77\ \mathrm{K}}-1\right] , \quad (15)$$

where T_R and p_R are room temperature and pressure. The target cell is then enclosed in an insulated cavity and cooled by the flow of helium gas from a liquid-helium dewar. Passing the cold gas ($T<8$ K) over the cell surface causes an increase of the ^{3}He density in the cell, and a decrease in the warm part of the manifold. The temperature of the cell is measured to an accuracy of ± 1 K at $T=10$ K by two independent silicon diode thermal resistors. As the cell is cooled, the pressure in the manifold drops below atmospheric pressure, which ensures that the capillary will seal itself when the cell is pulled from the manifold by melting the capillary with a flame. The final cell pressure at 273 K is then given by $p_{273}=(273\ \mathrm{K}/T_c)p_c$, where T_c is the temperature of the cold cell at the moment the capillary is sealed, and p_c is the pressure measured by the transducer. In practice temperature fluctuations encountered while the cell is being pulled off by application of the flame render a direct temperature reading inaccurate. Instead, the effective cell temperature at pulloff is determined from

$$T_C=\frac{T_R p_c f}{p_S-(1-f)p_C} , \quad (16)$$

where p_S is the pressure at room temperature. The relative density p can thus be obtained to an accuracy of $\pm 2\%$. The pressures for some of our best cells are given in Table II together with wall relaxation times Γ_w^{-1}.

The cells are heated to ~ 450 K in an oven made of the polyimide Vespel to produce Rb vapor of the required number density $[\mathrm{Rb}]\approx 4\times10^{14}$ cm^{-3}. The oven has a distributed heat flow around the cell which can be finely adjusted. This was necessary to reduce temperature gradients over the cell volume which introduce large uncertainties in [Rb]. Care was taken that the temperature variation did not exceed 3 K over the full cell surface. An uncertainty of ± 1.5 K at 453 K implies a 6% uncertainty in the Rb number density.

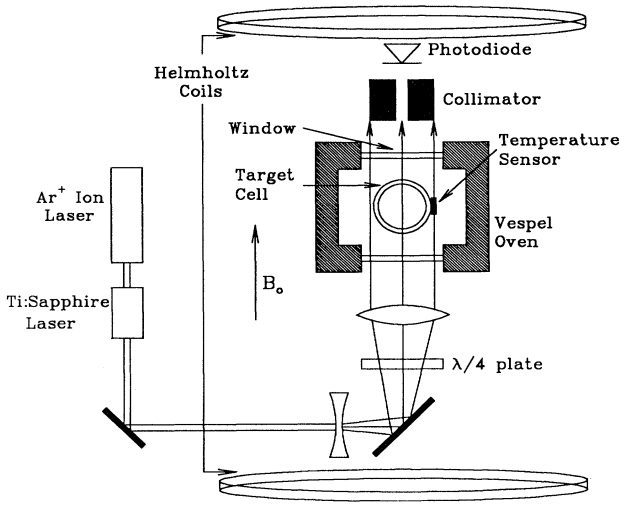

FIG. 2. Experimental setup for measurements of light transmission through ^{3}He target cells.

A parallel beam of infrared light from a frequency tunable Ti:sapphire laser was used to uniformly illuminate the cylindrical glass cells perpendicular to the 8-cm long cell axis (see Fig. 2). The Ti:sapphire laser is continuously pumped by a high power Ar^+ ion laser with $\sim$20–25 W of visible light. The efficiency of converting the Ar pump light into infrared light at 794.7 nm is $\sim$20%. We have two such systems running in parallel producing a combined power of $\approx$8–10 W of 795-nm light. For polarized target experiments the full available power is used, whereas for the transmission measurements the laser power was reduced to retain sensitivity to the spin-destruction rate, Γ_{SD}.

The laser linewidth ($\sim$18 GHz) is much smaller than the total absorption width Γ of the Rb $D1$ line which is dominated by pressure broadening. The laser line shape may therefore be considered a δ function for the purpose of calculating the frequency-dependent cross section [Eq. (2)] as was assumed in Sec. II. The average frequency of the infrared light was measured with a Burleigh WA-10 wavemeter. The transmitted light intensity was measured with a Newport 818-SL photodiode, calibrated for the frequency range of interest relative to two Coherent power meters which agreed to better than 2%. Collimation of the photodiode to a small area (0.07 cm^2) ensured that the light traversed nearly the full inner diameter of the glass cells. Measurements of the transmitted light intensities over a range of frequencies near the $D1$ resonance determine the Rb absorption line shape.

The frequency calibration of the Ti:sapphire laser could be checked frequently and conveniently by observing $D1$ and $D2$ resonance fluorescence in a reference cell which contained pure Rb vapor at $\approx$450 K. This was essential for measurements of the small pressure shifts of the $D1$ and $D2$ absorption maxima. Experimentally determined corrections were applied to the data to account for reflection, absorption, and refraction effects in the glass of the cell and of the entrance and exit windows of the oven in which it was mounted. Small corrections were also necessary to renormalize small frequency-dependent variations in the intensity of the incident light. Transmission scans were performed on four cells, each containing several mg of Rb metal, $\approx$120 Torr of N_2 quench gas (relative density $p=0.16$ atm) and ^{3}He gas of relative density $p=2.94$, 6.44, 8.97, and 12.1 atm, respectively (see Table I). The results obtained are presented in the following section. For scans with circularly polarized light a 3-mT holding field was applied along the direction of the incident light.

Measurements of γ_{SE} required that the cells be optically pumped for several hours to build up the ^{3}He polarization. The laser light was then blocked to follow the decay of the polarization. The bulk ^{3}He polarization could be analyzed and reversed using the nuclear magnetic resonance (NMR) technique of adiabatic fast passage (AFP) at a frequency of $\sim$100 kHz. At least two decay curves were measured for each cell: one at room temperature to determine the wall relaxation rate Γ_w, and one at $T\simeq$450 K to determine $\gamma_{SE}+\Gamma_w$.

Absolute normalization factors were obtained by comparing the ^{3}He AFP NMR signals (typically 0.3 V) with weak proton AFP NMR signals from water-filled cells of the same dimension (typically 1 μV). Our NMR setup is similar to the one described by Chupp *et al.* [17]. An independent check of the NMR method has recently been developed at TRIUMF [24]. The method is based on the special properties of the $^3\vec{\text{He}}(\vec{p},\pi^+)^4$He reaction and is sensitive only to ^{3}He in the beam-interaction region. Parity conservation in the strong interaction, channel spins 1 and 0 for entrance and exit channels, and parity change in the reaction, imply the identities $A_{nn}=1$ and $A_{n0}=A_{0n}$ for spin correlation parameter and beam- and target-related analyzing powers [25]. After determining the beam-related analyzing power A_{n0} for 416-MeV polarized protons at a laboratory scattering angle of 28°, absolute ^{3}He polarizations were obtained to an accuracy of $\pm$0.02. The absolute ^{3}He polarization results from the reaction method are in good agreement with the AFP

TABLE I. Light absorption parameters for the Rb $D1$ line.

^{3}He pressure (atm)	x (cm)	$\nu_0(p)-\nu_0(0)$ (GHz)	Γ (GHz)	Γ_a (GHz)	b (10^{-12} s)	$\Gamma_{SD}/[\text{Rb}]$ (10^{-12}cm^{3}s^{-1})
2.94	1.68	14.3±1.9	54±3	154±11	0.20± 0.04	0.93±0.08
6.44	1.68	34.7±4.8	126±5	146±11	1.0±0.2	1.37±0.12
8.97	1.68	53.7±3.8	184±6	184±11	1.5±0.2	2.02±0.17
12.1	2.00	73.2±1.9	244±7	225±12	1.5±0.2	2.82±0.24

NMR measurements. The reaction method is more direct and less susceptible to systematic errors than NMR, but requires expensive accelerator time. The ^{3}He polarization results of the present work were obtained with the more readily available NMR method.

IV. RESULTS

A. Transmission data and average Rb polarization

Transmission scans performed with linearly polarized (σ_0) light at temperatures near 393 and 452 K are shown in Fig. 3. At $T=393$ K the Rb number density, [Rb] is sufficiently low that the transmitted intensity is measurable even on resonance. The data were fitted with the expression (2). From these scans the pressure shifts, pressure broadened widths, and asymmetry parameters were obtained for each of the four cells.

The fits to the data shown in Fig. 3 were obtained with parameters Γ, Γ_a, and b given in Table I and with Rb number densities calculated from the vapor pressure formula of Killian [26]

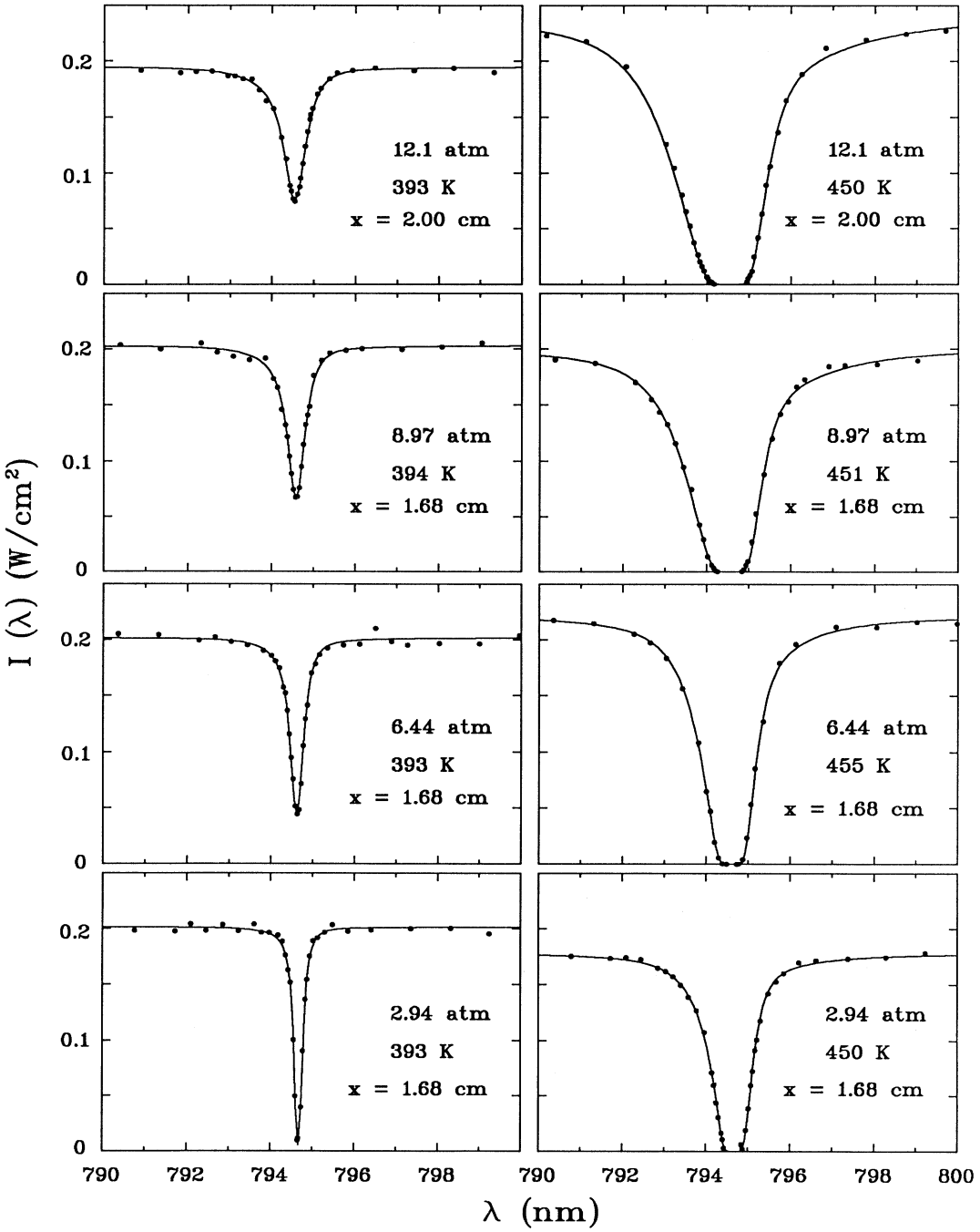

FIG. 3. Transmission of linearly polarized light through different cells at temperatures near 393 K (left) and 450 K (right). The solid curves are fits with Γ, Γ_a, and b from Table I.

$$\log_{10}[\mathrm{Rb}] = 26.41 - 4132/T - \log_{10} T \ . \quad (17)$$

When [Rb] is fitted as a free parameter, the values obtained agree with the calculated ones to better than 10%. The pressure shifts for the Rb $D1$ line are shown in Fig. 4 (top panel) together with an empirical fit, $\nu_0(p) - \nu_0(0) = (4.8p + 0.106p^2)$ GHz. Our values are systematically lower than the shifts measured for ^{4}He gas in earlier work by Ch'en [27]. This is to be expected since the shifts, in general, decrease with decreasing molecular weight [28]. The linewidth Γ (see Fig. 4, bottom panel) is found to increase linearly with ^{3}He pressure, i.e., $\Gamma = 20.0p$ GHz. This implies that the absorption length, $\kappa_{\nu_0}^{-1}(p) \approx 88p$ μm on resonance and for $[\mathrm{Rb}] = 4 \times 10^{14}$ atoms/cm^3, increases linearly with pressure. Our results are in approximate agreement with the measurements of Ch'en [27]. The linewidth does not seem to depend on molecular weight so our ^{3}He results should be directly comparable to the ^{4}He results of Ch'en.

Transmission scans performed with circularly polarized light are displayed in Fig. 5. The solid curves represent fits to the data with the use of Eq. (5)–(11) to calculate the transmitted light intensity and the average Rb polarization. The frequency dependence of the absorption cross section is given by Eq. (2) where the asymmetry parameters, pressure shifts, and widths are determined from the fits to the data obtained with linearly polarized light. The line-shape data obtained with circularly polarized light display a pronounced absorption spike near $\nu_0(p)$ which is likely caused by the presence of unpolarized Rb at the glass surface. The effective thickness of the layer of unpolarized Rb, l, is given approximately by $l = [D/(\gamma_v^+ + \Gamma_{\mathrm{SD}})]^{1/2}$ [see Eq. (11)] where D is the effective diffusion constant for Rb in ^{3}He gas. We have fitted D with our one-dimensional model assuming that D varies inversely with ^{3}He pressure, i.e., $D = D_0/p$. We

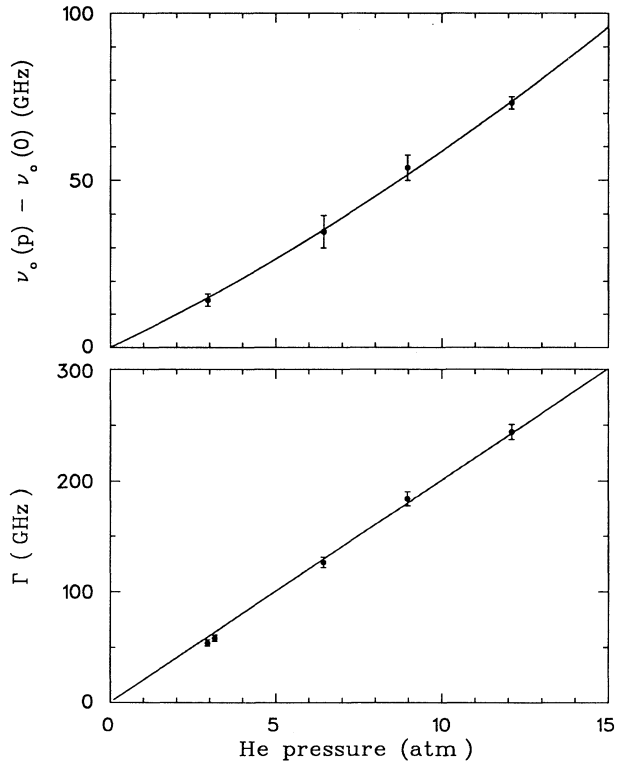

FIG. 4. Pressure shift of the Rb $D1$ line (top), and pressure broadening of the $D1$ line width Γ (bottom).

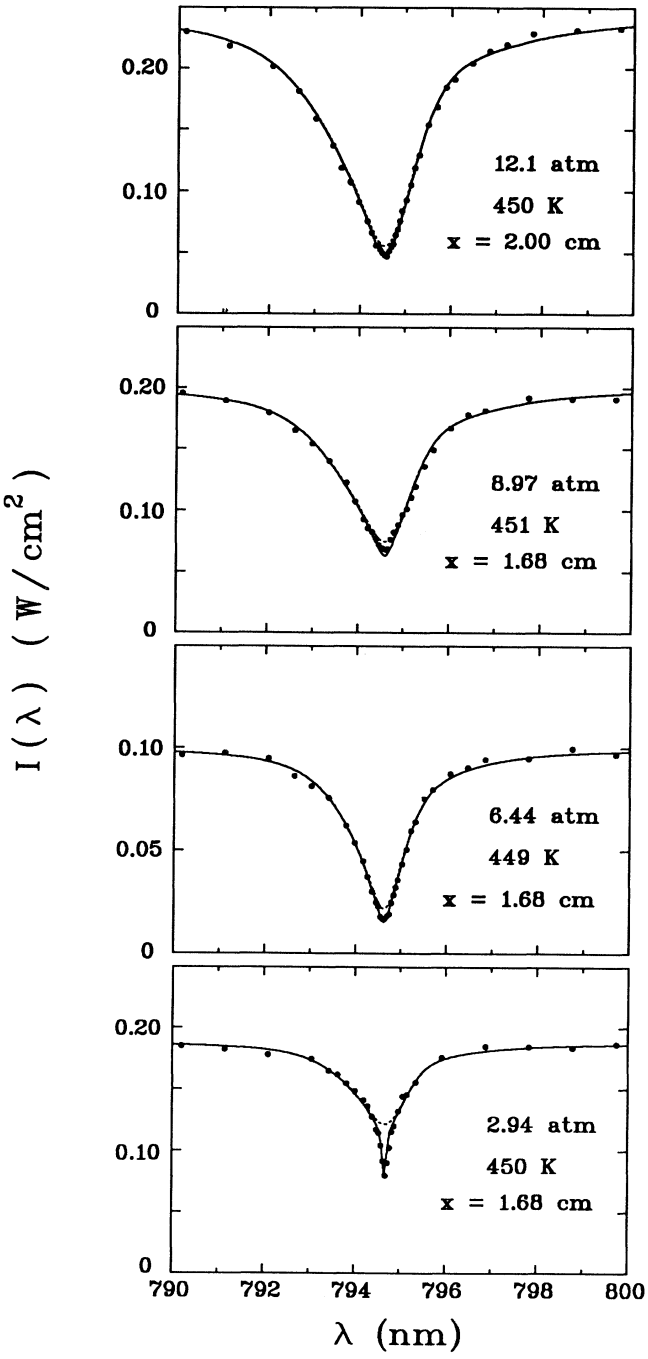

FIG. 5. Transmission scans at $T \approx 450$ K for circularly polarized light. The solid curves include a ≈ 40-μm thick unpolarized Rb layer at the glass surface, whereas the dotted curves were calculated without such a layer. The calculations use spin-destruction parameters shown in Table I.

find that a fixed value $D_0 = 3.5\ \mathrm{cm^2\,s^{-1}}$ gives acceptable fits for the range of pressures and light intensities used in our work. It should be noted that the fitted value is larger by about a factor of 6 than that quoted by Bernheim [29] for ^{4}He and Rb. The source of this discrepancy is unclear and may arise from the simplifying assumptions made in describing the physics of Rb depolarization near the cell wall. We have shown previously [30] that an elliptical polarization component of the light cannot produce such a sharp absorption spike and, furthermore, the ellipticity of the incident light was measured to be less than 5%. Evidence for the unpolarized layer is less compelling at higher pressures which is expected because of decreased diffusion at higher pressure.

Apart from the diffusion constant D_0, the spin-destruction rate Γ_{SD} is the only adjustable parameter needed to describe the transmission data. The fitted spin-destruction rates per Rb number density, $\Gamma_{SD}/[\mathrm{Rb}]$ in Table I, include the effect of unpolarized layers at the cell walls described by Eq. (11). The dependence of the ratio $\Gamma_{SD}/[\mathrm{Rb}]$ on ^{3}He pressure is shown in Fig. 6 (top panel) together with a value determined by Knize and Happer [31] who used the time-dependent method. We assume that the spin-destruction rate can be described by

$$\Gamma_{SD} = \langle \sigma_{SD} v \rangle [\mathrm{Rb}] + \langle \sigma_{SE} v \rangle [^3\mathrm{He}] + k[^3\mathrm{He}]^2 . \quad (18)$$

Spin destruction due to the presence of N_2 gas is ignored because the N_2 pressure is low (120 Torr) and constant. Fitting the data using the ^{3}He relative density p in place of the number density we obtain

$$\Gamma_{SD} = 325.0 + 1.64p + 5.44p^2\ \mathrm{s^{-1}} \quad (19)$$

at $[\mathrm{Rb}] = 4\times10^{14}\ \mathrm{cm^{-3}}$. The constant term probably arises from spin destruction during Rb-Rb collisions as has been assumed previously (see Ref.[17]). We have confirmed this by additional measurements shown in Fig. 6 (bottom panel) in which [Rb] was varied at a ^{3}He buffer gas pressure $p = 12.1$ atm. The data have been fitted with the expression $\Gamma_{SD} = a \times [\mathrm{Rb}] + b$. The parameter a represents the velocity averaged rate constant for spin destruction in Rb-Rb collisions. We find that this value is $(8.3 \pm 0.6)\times10^{-13}\ \mathrm{cm^3 s^{-1}}$ in good agreement with earlier measurements by Knize and Happer [31] at lower ^{3}He densities. The parameter b represents Rb spin destruction induced by ^{3}He and N_2.

The linear term in Eqs. (17) and (18) represents mainly Rb spin relaxation due to spin exchange with ^{3}He nuclei. The multiplier is calculated using the measured Rb-^{3}He spin-exchange rate (see below). At high ^{3}He densities the spin-destruction rate per Rb atom due to Rb-^{3}He exchange becomes significant but not large. The Rb-Rb and the Rb-^{3}He spin-destruction rates are shown as the dashed lines in the top panel of Fig. 6.

The quadratic term in Eqs. (17) and (18) suggests polarization losses initiated by three-body collisions of a Rb atom with two ^{3}He atoms. For heavier noble gases (Ar, Kr, Xe) at lower pressures ($\approx 1-100$ Torr) such collisions have been shown [32,15,16] to result in the formation of van der Waals molecules, with the third collision partner required to carry away the binding energy of the

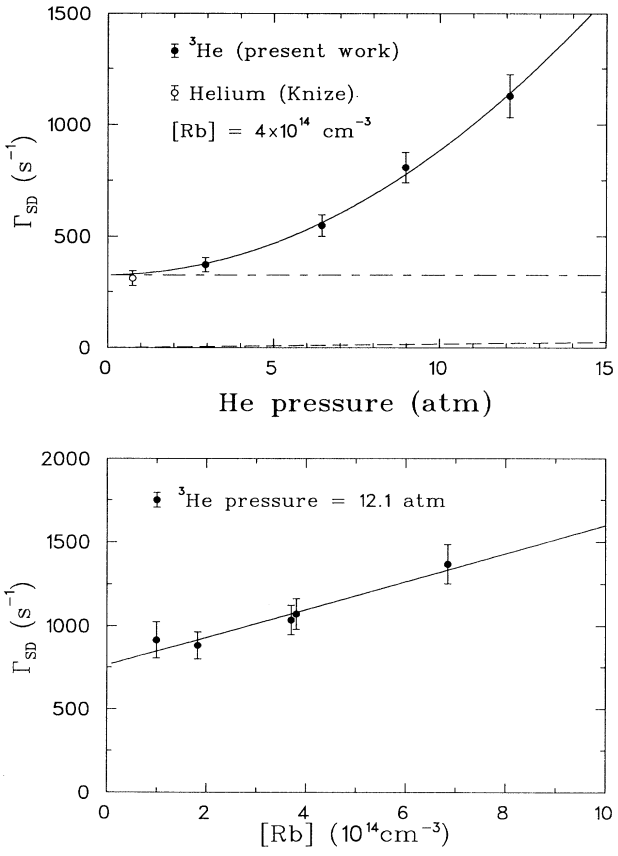

FIG. 6. The dependence of the spin-destruction rate Γ_{SD} on ^{3}He pressure (top panel). The solid curve represents the total measured spin-destruction rate, the dot-dashed curve is the assumed constant Rb-Rb contribution, and the dashed curve is the spin destruction arising from spin exchange between Rb and ^{3}He. The dependence of Γ_{SD} on Rb density at $p = 12.1$ atm is shown in the lower panel.

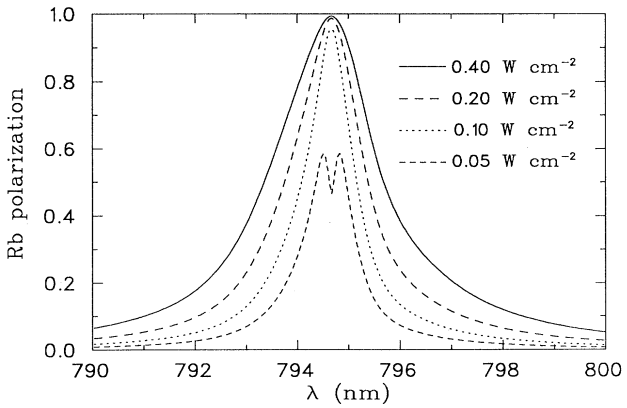

FIG. 7. Rb polarization in a 2-cm long cell predicted for various light intensities. The Rb density was assumed to be $4\times10^{14}\ \mathrm{cm^{-3}}$.

molecule. Destruction of the Rb spin in the molecule is caused by the spin-rotation interaction between the electron spin of the Rb and the rotational angular momentum of the molecule, as was first shown by Bernheim [29]. The molecular formation rate $T_F^{-1}=\delta p^2$ is expected to be proportional to the square of the noble-gas pressure, where δ is some constant. However, the spin-destruction rate is expected [15,16] to level off at high pressure as

$$\Gamma_{\rm SD}^{\rm mol}=\delta\frac{2}{3}\frac{p^2}{1+(p/p_0)^2}\ , \tag{20}$$

where p_0 is a characteristic pressure (typically 10–100 Torr) at which the mean spin rotation angle is 1 rad. In previous work such molecules have typical lifetimes of 10^{-8} s, limited by the binary collision rate, thus allowing a large spin rotation angle. In the present work the very short time between binary collisions (1–10 ps) implies rapid breakup of any Rb-^{3}He molecules; however a sizable spin rotation angle may still accumulate stochastically between absorption of subsequent photons.

Our success in quantitatively describing the transmission data of Figs. 3 and 6 implies that we can predict reliably the average Rb polarization in the cell volume. As an example Fig. 7 shows $P_{\rm Rb}$ for a 2-cm long cell at $p=3$ atm, $[{\rm Rb}]=4\times10^{14}$ cm^{-3}, and four different laser powers. For the lowest laser power $P_{\rm Rb}$ exhibits a dip on resonance $[\nu_0(p)]$ which is caused by the enhanced light absorption near the cell walls. At higher laser powers it is most efficient to pump at the resonance frequency. Modulation of the laser frequency, a method commonly used in laser spectroscopy to overcome "hole-burning", is not applicable in the high-pressure regime. The high frequency of Rb-^{3}He collisions, estimated to be $\tau_{\rm coll}^{-1}\approx1.9p\times10^{10}$ Hz, ensures that the absorption profile is fully reestablished in the time interval between absorption of subsequent photons.

Finally we discuss the question of laser power required to optically pump Rb at various ^{3}He pressures. The strong increase of the spin-destruction rate versus p makes it unfavorable to optically pump Rb at high pressures. We have calculated the laser power required at the resonance frequency $\nu_0(p)$ to pump a typical number density $[{\rm Rb}]=4\times10^{14}$ cm^{-3} to an average polarization of 96%. The calculations include the effects of the unpolarized layer at the entrance and exit walls of the glass cell. Results for various cell thicknesses x (in cm) are shown in Fig. 8 together with an empirical fit

$$I(\nu_0(p))=[39.6+0.551(p-3)p]\times\left[x+0.27\frac{p}{x^{1/2}}\right]\ {\rm mW\,cm^{-2}}\ . \tag{21}$$

This estimate, which is supported by our transmission results for $x=1.68$ and 2.0 cm, and for $p=3$–12 atm, has to be considered a *lower limit* because additional power is required in practice to compensate for nonuniformity of irradiation, frequency detuning, and losses incurred in the expansion and transport of the laser beam.

B. Rb-^{3}He spin-exchange measurements and ^{3}He polarization

The rate of Rb-^{3}He spin exchange has been determined from the decay of the ^{3}He polarization following laser irradiation for at least 12 h. For each cell the polarization decay measurements were repeated at various cell temperatures, from $T\approx453$ K ($[{\rm Rb}]\sim4.3\times10^{14}$ cm^{-3}) to room temperature (293 K). A typical set of decay measurements is presented in Fig. 9. The relative polarization is the AFP NMR signal normalized to the value at the start of the decay measurement. The ^{3}He pressure in this cell was $p=8.97$ atm.

Values for $\gamma_{\rm SE}$ are shown in Table II for five cells containing ^{3}He densities $p=3$–12 atm. They are fitted well with a constant value for the velocity averaged spin exchange cross section, $\langle\sigma_{\rm SE}v\rangle=(6.1\pm0.2)\times10^{-20}$ cm^{3}s^{-1} corresponding to a decay rate of $(10.6\ {\rm h})^{-1}$ at $T=453$ K. This value is almost a factor of 2 smaller than that of Chupp *et al.* [17]. We note that extraction of $\langle\sigma_{\rm SE}v\rangle$

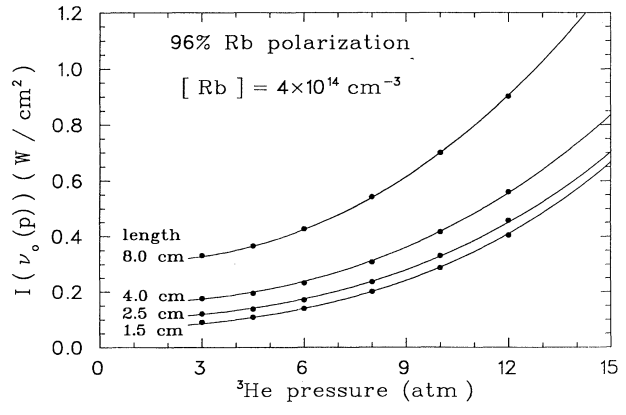

FIG. 8. Calculations of the laser power required to obtain 96% average Rb polarization in cells of various thicknesses. The curves represent an empirical fit described in the text.

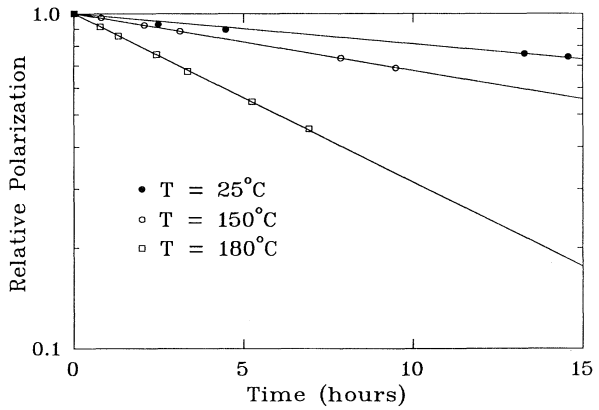

FIG. 9. Polarization decay curves for ^{3}He in the presence of various amounts of unpolarized Rb vapor.

TABLE II. Characteristic Rb-^{3}He spin-exchange times γ_{SE}^{-1} for [Rb]$=4\times10^{14}$ cm^{-3} and wall relaxation times Γ_w^{-1}.

^{3}He pressure (atm)	γ_{SE}^{-1} (h)	Γ_w^{-1} (h)
2.94	10.8±0.5	28.4±0.3
6.44	10.6±0.5	46.0±2.2
7.03	9.8±0.5	63.5±7.6
8.97	10.7±0.5	48.6±1.5
12.1	11.1±0.6	25.0±0.3

from the data requires an accurate knowledge of the Rb number density. As already mentioned in Sec. III we have paid special attention to the hot air flow around our cells to keep temperature gradients to typically ±1.5 K. Furthermore, we have obtained good consistency of [Rb] deduced from the transmission data (see Fig. 3) with those calculated by Killian's formula [26]. The cell wall relaxation rates, also shown in Table II, were determined at room temperature. A possible temperature dependence of Γ_w would modify the values of γ_{SE} extracted from the total decay rate, $(\gamma_{SE}+\Gamma_w)$, although the systematic error in γ_{SE} is likely to be small since the condition $\gamma_{SE}\gg\Gamma_w$ was generally fulfilled. Typical wall relaxation rates of cells used for in-beam experiments at TRIUMF are $\sim(50\text{ h})^{-1}$.

From Eq. (8), the maximum ^{3}He polarization obtainable with $P_{Rb}\approx1$,

$$\tilde{P}_{max}=\frac{\gamma_{SE}}{\gamma_{SE}+\Gamma_w} \tag{22}$$

is then approximately equal to 0.83. Using 8–9 W of laser light on cells of 17-cm^3 volume we have observed polarizations of 0.79 at $p=6.44$ atm (calculated $\tilde{P}_{max}=0.86$), and 0.73 at $p=8.97$ atm (calculated $\tilde{P}_{max}=0.82$). The difference between observed and calculated polarizations can probably be attributed to partial shadowing of the incident laser beam (Vespel fingers used to hold the glass, solid Rb droplets on the glass walls), and to diffraction effects of the incident light on the curved glass walls. With a cell of larger volume (35 cm^3) and at $p=7.03$ atm we have observed ^{3}He polarizations approximately equal to 0.55. We attribute this considerably smaller value to the difficulty of expanding the laser light uniformly over a large rectangular area (3×8.5 cm^2).

V. SUMMARY

Polarized ^{3}He targets of relative density $p=3-12$ atm have been built and tested. Transmission data with linearly polarized light near the Rb $D1$ frequency have been analyzed to determine the pressure broadened line shape (shift, width, and asymmetry) and the Rb number density. Transmission data with circularly polarized light contain evidence for a strong increase of the Rb spin-destruction rate with pressure which suggests the importance of three-body collisions. Absorption spikes near the resonance frequency provide evidence for the existence of a thin (≈40 μm) unpolarized layer at the glass boundary. The laser power required to achieve 96% Rb polarization has been estimated for a variety of pressures and geometries. Whereas the pressure broadening has only a minor effect on the required laser power the strong increase of Γ_{SD} with ^{3}He pressure necessitates a large increase in laser power. It is thus unfavorable to optically pump Rb vapor at high ^{3}He density.

The rate for Rb-^{3}He spin exchange was measured and found to be significantly lower than previously determined values. Maximum ^{3}He polarizations of 0.72–0.79 were observed at pressures $p=6-9$ atm. These polarization values are 85–90 % of the theoretical upper limits calculated for idealized conditions.

ACKNOWLEDGMENTS

The authors are indebted to T. E. Chupp, A. Gallagher, and W. Happer for helpful discussions. This work was supported by grants from the Natural Sciences and Engineering Research Council of Canada.

*Permanent address: National Accelerator Centre, Faure, 7131, South Africa.

[1] M. Leduc, J. Phys. (Paris) Colloq. **51**, C6-317 (1990).
[2] J. L. Friar, B. F. Gibson, G. L. Payne, A. M. Bernstein, and T. E. Chupp, Phys. Rev. C **42**, 2310 (1990).
[3] C. E. Woodward *et al.*, Phys. Rev. Lett. **65**, 698 (1990).
[4] K. P. Coulter, A. B. McDonald, W. Happer, T. E. Chupp, and M. Wagshul, Nucl. Instrum. Methods A **288**, 463 (1990).
[5] R. T. Johnson, D. N. Paulson, R. P. Giffard, and J. C. Wheatley, J. Low-Temp. Phys. **10**, 35 (1973).
[6] F. D. Colegrove, L. D. Schearer, and G. K. Walters, Phys. Rev. **132**, 2561 1963).
[7] R. G. Milner, R. D. McKeown, and C. E. Woodward, Nucl. Instrum. Methods A **274**, 56 (1989).
[8] M. A. Bouchiat, T. R. Carver, and C. M. Varnum, Phys. Rev. Lett. **5**, 373 (1960).
[9] R. L. Gamblin and T. R. Carver, Phys. Rev. **138**, 964 (1965).
[10] R. M. Herman, Phys. Rev. A **137**, 1062 (1965).
[11] B. C. Grover, Phys. Rev. Lett. **40**, 391 (1978).
[12] C. H. Volk, T. M. Kwon, and J. G. Mark, Phys. Rev. A **21**, 1549 (1980).
[13] N. D. Bhaskar, W. Happer, and T. McClelland, Phys. Rev. Lett. **49**, 25 (1982).
[14] N. D. Bhaskar, W. Happer, M. Larsson, and X. Zeng, Phys. Rev. Lett. **50**, 105 (1983).
[15] W. Happer, E. Miron, S. Schaefer, D. Schreiber, W. A. van Wijngaarden, and X. Zeng, Phys. Rev. A **29**, 3092 (1984).
[16] X. Zeng, Z. Wu, T. Call, E. Miron, D. Schreiber, and W. Happer, Phys. Rev. A **31**, 260 (1985).
[17] T. E. Chupp, M. E. Wagshul, K. P. Coulter, A. B. McDonald, and W. Happer, Phys. Rev. C **36**, 2244 (1987).

[18] M. E. Wagshul and T. E. Chupp, Phys. Rev. A **40**, 4447 (1989).
[19] O. Häusser, J. Phys. (Paris) Colloq. **51**, C6-99 (1990).
[20] W. Demtröder, *Laser Spectroscopy* (Springer-Verlag, Berlin, Heidelberg, 1981), pp. 79–111.
[21] A. Gallagher, in *Proceedings of the Fourth International Conference on Atomic Physics, Heidelberg, 1974,* edited by G. zu Putlitz, E. W. Weber, and A. Winnacker (Plenum, New York, 1975), pp. 559–574.
[22] TRIUMF Annual Report, 1989 (unpublished).
[23] L. Krause, in *The Excited State in Chemical Physics* (Wiley, New York, 1975), pp. 267–316.
[24] O. Häusser *et al.* (unpublished).
[25] G. G. Ohlsen, Rep. Prog. Phys. **35**, 717 (1972); G. G. Ohlsen and P. W. Keaton, Jr., in *Proceedings of the Second International Conference on Polarized Targets,* edited by G. Shapiro (Lawrence, Berkeley, 1971), LBL-500, pp. 367–369.
[26] T. J. Killian, Phys. Rev. **27**, 578 (1926).
[27] S. Y. Ch'en, Phys. Rev. **58**, 1051 (1940).
[28] S. Y. Ch'en and M. Takeo, Rev. Mod. Phys. **29**, 20 (1957).
[29] R. A. Bernheim, J. Chem. Phys. **36**, 135 (1962).
[30] O. Häusser, B. Larson, C. Chan, and P. Delheij, TRIUMF Annual Report, 1989 (unpublished).
[31] R. J. Knize and W. Happer, Bull. Am. Phys. Soc. **30**, 866 (1985); R. J. Knize, Phys. Rev. A **40**, 6219 (1989).
[32] M. A. Bouchiat, J. Brossel, and L. C. Pottier, J. Chem. Phys. **56**, 3703 (1972).